Inflight proton activation and damage on a CdTe detection plane

N. Simões [a,b], J.M. Maia [c,a,*], R.M. Curado da Silva [a,b,**], S. Ghithan [a,b], P. Crespo [a,b], S.J.C. do Carmo [d], Francisco Alves [d,e], M. Moita [a,b], N. Auricchio [f], E. Caroli [f]

[a] *LIP-Laboratório de Instrumentação e Física Experimental de Partículas, Portugal*
[b] *Physics Department, University of Coimbra, Coimbra, Portugal*
[c] *Physics Department, University of Beira-Interior, Covilhã, Portugal*
[d] *ICNAS - Instituto de Ciências Nucleares Aplicadas à Saúde, University of Coimbra, Coimbra, Portugal*
[e] *IPC - Instituto Politécnico de Coimbra - Coimbra Health School, 3046-854 Coimbra, Portugal*
[f] *INAF-IASF-Bologna, Bologna, Italy*

A B S T R A C T

Future high-energy space telescope missions require further analysis of orbital environment induced activation and radiation damage on main instruments. A scientific satellite is exposed to the charged particles harsh environment, mainly geomagnetically trapped protons (up to ~300 MeV) that interact with the payload materials, generating nuclear activation background noise within instruments' operational energy range and causing radiation damage in detector material. As a consequence, instruments' performances deteriorate during the mission time-frame. In order to optimize inflight operational performances of future CdTe high-energy telescope detection planes under orbital radiation environment, we measured and analyzed the effects generated by protons on CdTe ACRORAD detectors with 2.56 cm^2 sensitive area and 2 mm thickness. To carry-out this study, several sets of measurements were performed under a ~14 MeV cyclotron proton beam. Nuclear activation radionuclides' identification was performed. Estimation of activation background generated by short-lived radioisotopes during one day was less than ~1.3×10^{-5} counts cm^{-2} s^{-1} keV^{-1} up to 800 keV. A noticeable gamma-rays energy resolution degradation was registered (~60% @ 122 keV, ~14% @ 511 and ~2.2% @ 1275 keV) after an accumulated proton fluence of 4.5×10^{10} protons cm^{-2}, equivalent to ~22 years in-orbit fluence. One year later, the energy resolution of the irradiated prototype showed a good level of performance recovery.

1. Introduction

The effects of orbital radiation environment induced nuclear activation and material damage on high-energy space telescope instruments require further analysis. Indeed, space missions' background noise calibration has been a complex task [1–3]. In particular semiconductor based detection planes require further space environment testing in order to improve new instrument design solutions' sensitivity in orbit, such as 3D semiconductor detection planes or Laue lens focal planes [4,5].

Orbit space environments are composed of multiple radiation fields (protons, electrons, ions, gamma-rays, etc.) that interfere with the detection plane operational performances in the X- and gamma-ray energy band. Most weather, observation and scientific satellites as well as the International Space Station are located in a LEO (Low Earth Orbit), at flight altitudes between 180 and 2000 km, since these orbits require less communication time-delay and provide easier access for repairing, replacing or new instrumentation implementation. Even though, satellites remain most of the time without intercept high energy particle belts in orbits below 2000 km, when crossing the SAA (South Atlantic Anomaly) they are exposed to high proton fluxes and instruments are generally turned-off. A high-energy telescope onboard a satellite in a typical LEO of, for instance, ~550 km altitude, ~30º inclination and ~96 min period (ASTRO-H type) [6], is exposed to geomagnetically trapped protons with energies between 1 and 300 MeV, with an average differential and integrated proton flux profile as represented in Fig. 1 [7–11]. This harsh space environment deteriorates the detector performance during the mission time-frame, such as its energy resolution, peak channel, leakage current, etc.
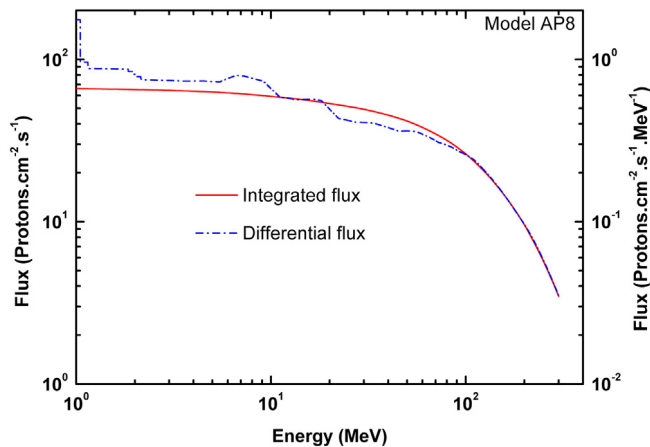
Fig. 1. Trapped proton integrated and differential average flux in a typical LEO (∼550 km altitude, ∼30º inclination and ∼96 min period) up to 300 MeV, calculated with OMERE 4.2 [11].

Fig. 2. The cathode view of the ACRORAD 8×8 CdTe detector inside a metallic shielded box that was closed by a metal cover with an entrance window of 20 mm diameter and 20 μm thick Al foil.

In such LEO, protons are the main source of nuclear activation of the detector materials generating a high-energy photon background noise from activation products' decay. Besides, the detector performance such as the energy resolution can be seriously affected by radiation damage caused by these protons.

LIP (Laboratório de Instrumentação e Física Experimental de Partículas), Coimbra, Portugal is a partner of AHEAD (Activities in the High Energy Astrophysics Domain) Horizon 2020 project (INFRAIA-2014-2015, ref.: 654215). The main objective of AHEAD is to promote synergies between the individual national efforts in high-energy astrophysics in order to set up future X- and gamma-ray telescope joint proposals with increased maturity to forthcoming ESA calls. Although the work herein described is not part of LIP tasks in AHEAD, it will provide complementary contribution for in-orbit performances optimization of future high-energy detection planes that may arise from AHEAD. With this scope, we studied and analyzed both the radiation damage effects and the nuclear activation of an ACRORAD CdTe prototype under a proton beam. Indeed, CdTe is a suitable material for main instrument detection plane due to its high resistivity (∼10^9 Ω cm) and band gap energy (∼1.44 eV) that allows low leakage current and room temperature operation. Its high average atomic number (Cd:48; Te:52) and high density (5.85 g/cm^3) offers the advantage of an excellent gamma-ray detection efficiency up to ∼1 MeV. However, the disadvantage is a higher nuclear activation background within the 100 keV up to 1 MeV energy range due to the high cross-sections of (p, xn) nuclear reactions for its high-Z target nuclei when irradiated by protons with energy between 1 and 100 MeV [12].

In order to study and analyze the effects generated by orbital trapped radiation, space instrument prototypes can be efficiently tested in accelerator radiation beams. Radiation damage experiments induced by a few monochromatic proton beams were previously performed, reporting a good CdTe radiation hardness for typical orbital environment proton fluences at 2, 15, 150, 200 and 300 MeV [13–16] as well as at combined beam energies between 10 and 200 MeV, however with limited conclusions on radiation damage [17]. One of these experiments monitored the induced activation on CdTe [16] for 150 MeV protons. Separately, proton induced nuclear activation on natural Cd [18,19] and on natural Te [20] were also analyzed, reporting the cross sections per nucleus versus proton energy for the formation of several radionuclides.

The CdTe prototype operated in this experiment was irradiated by a ∼14 MeV proton beam provided by ICNAS Cyclotron (*Instituto de Ciências Nucleares Aplicadas à Saúde*), University of Coimbra, Portugal. Such a proton beam is fairly representative of proton space environment, since LEO trapped proton flux is greater for such lower proton
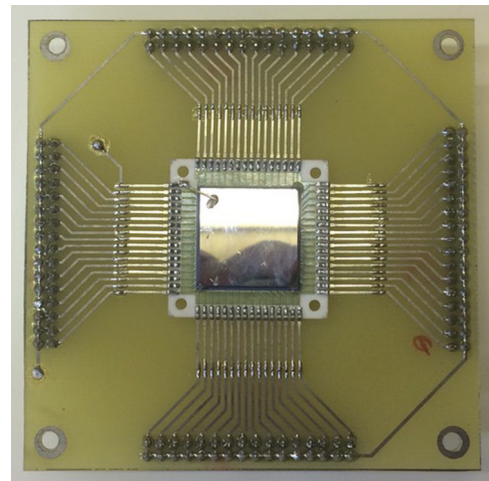
energies (Fig. 1). The analysis of the radiation hardness and of the nuclear activation induced background noise on CdTe detectors is herein addressed and discussed. Although, neutron production also contributes to the detector damage and activation, in this experiment we did not differentiate its effects on the detector from the remaining ones.

2. Experimental setup

To carry out this study, several tests were performed at ICNAS cyclotron facility irradiating several CdTe detectors by a ∼14 MeV proton beam. The detectors were 2.0 mm thick ACRORAD ohmic CdTe matrices with 8×8 pixels, each pixel with 1.9×1.9 mm^2 and 0.1 mm gap between consecutive pixels (Fig. 2), for a total 2.56 cm^2 sensitive area. In the segmented side, the electrodes (anodes) were composed by Au/Ni/Au/Pt while on the crystal opposite side the contact electrode was a 300 nm thickness layer of Pt. The output signals were processed by a Canberra 2003BT charge preamplifier, a Tennelec TC243 linear amplifier (1 μs shaping-time and 150 gain) and a ORTEC Maestro multichannel analyzer.

External and internal measurements of the nuclear activation radioisotopes induced by the proton beam on the CdTe were performed. The external measurements were performed by an ORTEC HPGe detector, with 0.47% energy resolution at 511 keV. The HPGe detector was shielded by 10 cm thick Pb blocks with a ∼20 mm diameter aperture. The experimental setup was installed in ICNAS underground facilities within concrete wall rooms.

ICNAS cyclotron can generate a proton beam with ∼150 μA (∼9.4×10^{14} protons/s) maximum current and 18 MeV maximum nominal energy, at the output of cyclotron yoke [21]. After leaving the cyclotron yoke, the proton beam crosses a 2.4 m long aluminum pipe divided into two segments with 0.4 m (at 10^{-5} bar) and 2.0 m (at 10^{-2} bar) in length, delimited at the ends by two 50 μm thick Havar windows (see Fig. 3). In front of the tube output, an aluminum collimator with variable diameter (0.5–23 mm range) directs the beam onto a 20 μm thick aluminum foil, that monitors the proton beam intensity current in the target (see methodology in [21]). The proton flux is controlled by an aluminum disk (150 mm radius) with a 0.5 mm slit that crosses the beam trajectory to the detector target, whose rotation frequency is controlled by a computer homemade program [21]. Finally, a computer-controlled shutter is placed before the target. The resulting proton beam is an almost monochromatic ∼14 MeV beam, tuned to generate fluences comparable to a typical LEO total fluence throughout a typical mission lifetime, i.e. up to ∼10^{10} protons/cm^2.
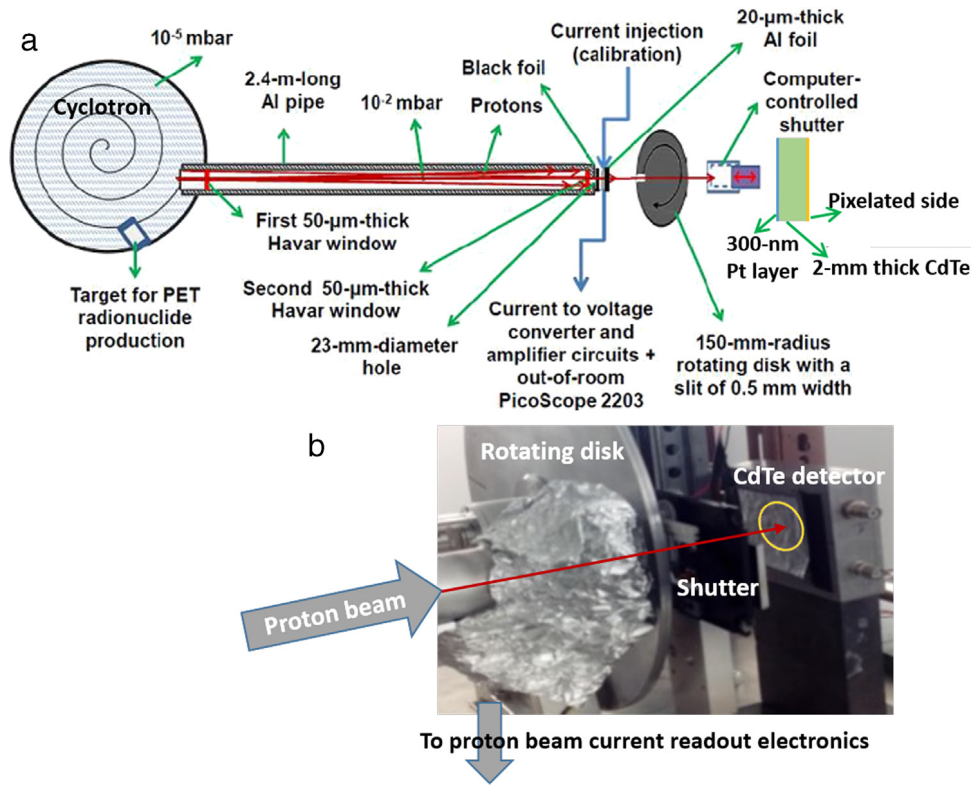
Fig. 3. (a) Schematic view of ICNAS cyclotron proton irradiation and mechanical setup to collimate and tune the proton beam onto the CdTe matrices. The protons dispersion in the first 50 µm thick Havar window is illustrated by the indicated paths, justifying the lateral straggling of the proton beam at the outlet of the aluminum tube. (b) Detail of the last stage of the proton irradiation setup [21].

3. CdTe nuclear activation background

High-Z CdTe target nucleus activation is generated by (p, xn) nuclear reaction high cross-section within the 1 to 100 MeV energy range [12,18–20]. Different types of nuclear reactions are likely to occur inside CdTe crystals for 14 MeV protons resulting from proton energy threshold of competing nuclear reactions and to the isotopic composition of natural Cd ([106]Cd:1.25%, [108]Cd:0.89%, [110]Cd:12.49%, [111]Cd:12.80%, [112]Cd:24.13%, [113]Cd:12.22%, [114]Cd:28.73%, [116]Cd: 7.49%,) and of natural Te ([120]Te:0.096%, [122]Te:2.603%, [123]Te:0.908%, [124]Te:4.816%, [125]Te:7.139%, [126]Te:18.95%, [128]Te:31.69%, [130]Te:33.8%). For the same isotope, reactions (p, xn) with higher x number of neutrons show higher energy thresholds [18–20], thus in our experiments only reactions with x = 1, 2 neutrons could be observed. Therefore, 14 MeV protons induce nuclear activation reactions on the natural isotopes of Te and Cd, producing mainly radioisotopes of Iodine and Indium, respectively, accompanied by the emission of 1 or 2 neutrons. Some of the decay modes of these radioisotopes generate gamma-rays with energy mostly within the 100 to 1000 keV range, contributing to the background noise in the operational energy range of a CdTe detection plane. Further possible decay modes are the isobaric transformations (β^- decay, β^+ decay or EC: electron capture) and the isomeric transformations (excited states, metastable states or IT: internal conversion). These decay modes generate electron or positron continuum emission spectrum followed by gamma-ray line emissions (such as 511 keV), as well as primary gamma-ray line emissions or internal conversion electron emissions with several discrete energies.

Since ICNAS proton beam irradiation setup (Fig. 3) limits output proton energies up to 14 MeV, it is not possible to reproduce the orbital proton energy profile in a LEO up to a few hundreds of MeV (Fig. 1). However, 14 MeV lay in the energy band where the orbital proton flux is more intense as shown in Fig. 1. Besides, the nuclear activation reactions cross-sections with the isotopes of Cd and Te [18–20] are strongly dependent on proton energy, above the (p, n) reactions

thresholds (typical 1–6 MeV), displaying a sequence of maximum and minimum as the energy increases and the other competitive nuclear reaction channels comes into play, e.g. (p, 2n), (p, 3n), etc., starting to decline steadily, for the majority of the isotopes, for energies above ~50 MeV, and becoming very low for higher energies, up to hundreds of MeV. When considering the range up to ~300 MeV (Fig. 1), the average cross section in this band is about of the same order of magnitude as the cross section for ~14 MeV [18–20]. Therefore, simulation of in-orbit proton irradiation effects with a ~14 MeV proton beam with a total fluence level of the order of the real LEO orbit total proton fluence within 1 to 300 MeV, should be fairly representative of most proton activation during a typical LEO mission. It stands for a good balance when considering overall flux and cross-sections profiles.

To calculate the 14 MeV proton beam energy deposit inside the CdTe detector, a set of simulations was performed with SRIM/TRIM toolkit [20]. A point source proton beam transversally irradiating the 300 nm Pt layer side of a 2.0 mm thick CdTe crystal was simulated. The stopping power, $-\frac{dE}{dx}$, versus the penetration depth (Bragg curves) is represented in Fig. 4. For protons with a mean range up to 2 mm (up to 25 MeV protons), the activation nuclear reactions cross-section varies with the CdTe crystal depth (Fig. 4). The energy loss per unit length decreases with the as the proton energy increases. At 14 MeV, protons' mean range in CdTe is 0.81 mm. For protons with a mean range over 2 mm (>25 MeV protons), the energy loss per unit length is relatively low and cross-sections remain approximately constant as well as the nuclear activation depth (2 mm full thickness). Again, using a 14 MeV proton beam appears as a balanced and representative choice considering the activation depth dependence.

3.1. External measurements

The CdTe detectors were mounted at the ICNAS cyclotron proton setup (Fig. 3) and were then irradiated from Pt layer side by an

Table 1
Proton beam (~14 MeV, ⌀18 mm) irradiation settings for nuclear activation of the CdTe matrix.

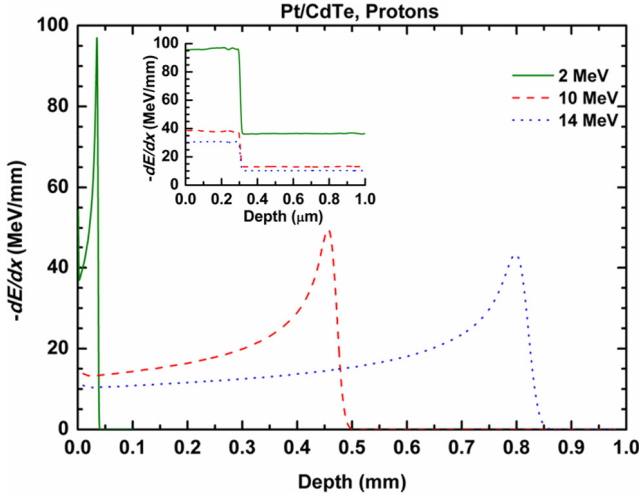|	Irradiation A_1	Irradiation A_2	Irradiation A_3
Flux (protons cm^{-2} s^{-1})	4.1×10^7	2.3×10^8	2.7×10^{11}
Irradiation time (s)	120	200	200
Fluence (protons cm^{-2})	4.92×10^9	4.60×10^{10}	5.40×10^{13}
Total fluence (protons cm^{-2})	4.92×10^9	5.09×10^{10}	5.41×10^{13}
End of beam time	06/07/15	07/07/15	09/07/15
	19 h 34 min 25 s	19 h 47 min 00 s	20 h 41 min 20 s

Fig. 4. Energy loss per unit length by a proton beam (for 2 MeV, 10 MeV and 14 MeV), within a 2 mm thick CdTe crystal, computed with SRIM/TRIM simulation toolkit [22]. The inset zoom represent the energy loss in the 300 nm Pt layer in the boundary region.

18 mm diameter uniform proton beam with ~14 MeV, according to the irradiation sequence described in Table 1. This irradiation sequence was implemented to study and analyze the gamma-rays generated by nuclear activation reactions, mainly via (p, xn) reactions on a passive (not polarized) CdTe matrix. Following each irradiation, the activated CdTe matrix was removed from the cyclotron bunker (after being guaranteed radiological safety: tens of minutes after irradiations A_1 and A_2 up to a few hours of cooling time after irradiation A_3) and placed in the HPGe setup. Then, the gamma-ray spectra were acquired during a time-frame of several minutes up to a few hours, after the end of beam time proton irradiation (Fig. 5).

In Tables 2 and 3 are summarized the main indium and iodine radioisotopes identified generated by natural isotopes of Cd and Te, in decreasing order cross-sections [18–20,23,24]. Additionally, the referred tables show the radionuclides half-life, $T_{1/2}$, the decay modes and yields, the decay products and the main gamma-ray lines energy with its yield per disintegration, I_γ.

Different acquisition times, allowed to determine the average activities of the different radioisotopes, identified via the main gamma-ray lines (Tables 2 and 3). Given the variability of the radionuclides half-life, $T_{1/2}$ (from a few seconds to over 1 year), it was not always simple or even possible to estimate from measurements the activity of a radioisotope. Thus, for A_1 irradiation we could identify and estimate the activity of main radionuclides with $T_{1/2}$ between 7.7 min and 1.66 h, for A_2 irradiation with $T_{1/2}$ between 7.7 min and 2.8 d, and for A_3 irradiation with $T_{1/2}$ between 1.66 h and 49.5 d. In Fig. 5 are shown the gamma-ray spectra obtained after A_2 and A_3 irradiations.

Simulations performed with OMERE software show that the A_2 irradiation represents ~20 years of proton accumulated fluence in the 1 to 300 MeV range for a LEO (550 km altitude, 96 min period, 30º inclination) similar to CdTe based ASTRO-H orbit (Fig. 1) [6]. 20 years is a reasonable estimation as maximum mission duration in the case of

a high-energy observatory mission − INTEGRAL is already operating in space for 14 years.

A_3 irradiation fluence is more than three orders of magnitude higher than the accumulated fluence in a LEO mission. In the case of A_3 the objective was not to compare with in-orbit fluence, but to generate enough nuclear activation in order to obtain sufficient gamma-ray statistics which would allow identifying the maximum number of activation peaks, especially those that although were not identified after A_2 irradiation but were hidden in these spectra and thus contribute to the in-orbit background noise.

These measurements allowed us to reveal tens of gamma-ray lines and thus identify most of the radionuclides. These are presented in Tables 2 and 3. In bold are reported the identified gamma-rays lines, E_γ, and the corresponding radionuclides. For A_2 irradiation, we identified the following radionuclides within the time-frame of ~10 min up to ~15 min after irradiation (Fig. 5a and 5b): ^{111m}Cd, ^{112m}In, ^{111}In, ^{111}In + ^{111m}Cd, ^{113m}In, ^{116m}In, ^{128}I, ^{111m}In, ^{112}In, ^{108m}In + ^{108}In, ^{110m}In + ^{110}In, ^{130}I, ^{110}In and ^{108m}In. Within the time-frame of ~1 h up to ~4.3 h after irradiation were identified: ^{123}I, ^{111}In, ^{109}In, ^{111}In + ^{111m}Cd, ^{115m}In, ^{113m}In, ^{116m}In, ^{130}I, ^{124}I, ^{110m}In + ^{110}In, ^{110}In, ^{108m}In and ^{116m}In. For A_3 irradiation were identified the following radionuclides within the period of ~5.0 h up to 5.6 h after irradiation (Fig. 5c and Fig. 5d): ^{123}I, ^{111}In, ^{109}In, ^{121}I, ^{115m}In, ^{113m}In, ^{130}I, ^{110}In, ^{124}I, ^{110m}In + ^{110}In, ^{126}I and ^{116m}In. Within the period of ~43.0 h up to 43.3 h after irradiation were identified: ^{123}I, ^{111}In, ^{114m}In, ^{126}I, ^{130}I, ^{124}I and ^{110}In.

3.2. Internal measurements

Complementary activation measurements were performed on nuclear activation induced background noise inside the irradiated CdTe prototype itself. These measurements provide further data on background generated by activation, including not only the gamma-ray activation emissions, as well as electron- and positron-emission continuum spectrum (β^- decay, β^+ decay) and internal conversion electron emission lines (Tables 2 and 3) [24].

After performing each proton irradiation (Table 4), the activated CdTe detector was removed from the cyclotron bunker after a cooling time of a few minutes and connected to the electronic readout chain. The CdTe detector was then polarized at 600 V. The spectra generated by the internal activation, between 15 and 45 min after irradiation, are shown in Fig. 6. As expected, we found fewer gamma-ray peaks compared with external measurements, due to the energy internal continuous spectra of electrons and positrons and to the worst CdTe detector energy resolution (~12.5% at 122 keV and ~4.5% at 511 keV). For the Irradiation 1 we identified the radionuclides ^{112m}In, ^{113m}In and ^{111m}In (Fig. 6a), while for Irradiation 4 the radionuclides ^{112m}In, ^{113m}In, ^{111m}In and ^{115m}In were identified (Fig. 6b). Furthermore, a new peak arises, to the left of the 156.6 keV gamma-rays line of the ^{112m}In, with ~129 keV energy which could be credited to the ^{112m}In-K internal conversion electrons, being its yield per disintegration of ~66.7% [24]. The observed internal activation spectra of the CdTe detector showed a steady decrease of the activation background with the energy, despite a few small peaks and the prominent 156.6 keV energy peak. After Irradiation 4, the background level recorded (except 156.6 keV peak) went from ~10^{-1} at 100 keV, down to 2×10^{-2} counts/cm^2 s keV at 800 keV.

Table 2

Characteristics of the main indium radioisotopes generated by the irradiation of natural Cadmium by 14 MeV protons, ordered by decreasing cross-sections - . Whenever the decay daughter-nuclide is not stable, its characteristics are also presented.

Radioisotope	Half-life, $T_{1/2}$	Decay-mode (%)	Energy, E_γ (keV)	Yield per disintegration, I_γ (%)	Nuclear reactions	Threshold (MeV)
^{111}In → ^{111}Cd	2.80 d	EC (100)	**171.3**	90.7	^{111}Cd (p, n)	1.66
			245.4	94.1		
^{111m}In	7.7 min	IT (100)	**537.0**	87.2	^{112}Cd (p, 2n)	11.14
^{110m}In → ^{110}Cd	69.1 min	EC, β^+ (100)	511.0	122.5	^{110}Cd (p, n)	4.70
			657.8	97.7		
^{110}In → ^{110}Cd	4.92 h	EC (100)	**461.5**	7.4	^{111}Cd (p, 2n)	11.74
			581.9	8.6		
			584.2	6.5		
			641.7	26.0		
			657.8	98.0		
			677.6	4.5		
			707.4	31.2		
			759.9	3.2		
			844.7	3.2		
			884.7	93.0		
			901.5	2.0		
			937.5	68.4		
			997.3	10.5		
			1117.4	4.2		
^{112}In → ^{112}Cd	14.97 min	EC, β^+ (57)	**617.5**	1.0	^{112}Cd (p, n)	3.40
			511.0	46.7		
→ ^{112}Sn		β^- (43)	–	–	^{113}Cd (p, 2n)	10.0
^{112m}In	20.56 min	IT (100)	**156.6**	13.3		
^{113m}In	1.66 h	IT (100)	**391.7**	64.9	^{113}Cd (p, n)	0.47
					^{114}Cd (p, 2n)	9.59
^{114m1}In → ^{114}In	49.51 d	IT (96.8)	**190.3**	15.6	^{114}Cd (p, n)	2.25
→ ^{114}Cd		EC (3.2)	558.4	4.4		
			725.2	4.4		
^{114}In → ^{114}Sn	71.9 s	β^- (99.5)	–	–		
^{115m}In → ^{115}In	4.49 h	IT (95.0)	**336.2**	45.8	^{116}Cd (p, 2n)	8.11
→ ^{115}Sn		β^- (5.0)	–	–		
^{116m1}In → ^{116}Sn	54.29 min	β^- (100)	138.3	3.7	^{116}Cd (p, n)	1.26
			416.9	27.2		
			818.7	12.1		
			1097.3	58.5		
			1293.6	84.8		
^{116m2}In → ^{116m1}In	2.18 s	IT (100)	162.4	37.2		
^{116}In → ^{116}Sn	14.10 s	bbr β^- (100)	1293.4	1.30		
^{109}In → ^{109}Cd	4.167 h	EC, β^+ (100)	**203.5**	73.5	^{110}Cd (p, 2n)	12.83
			426.2	4.1		
			511.0	9.1		
			623.5	5.5		
			1149.1	4.3		
^{109}Cd → ^{109}Ag	461.4 d	EC (100)	88.0	3.7		
^{109m1}In	1.34 min	IT (100)	650.1	93.7		
^{109m2}In	0.209 s	IT (100)	402.2	21		
			673.5	100		
			1025.3	25		
			1427.5	75		
^{108m}In → ^{108}Cd	39.6 min	EC, β^+ (100)	511.0	100.8	^{108}Cd (p, n)	5.99
			632.9	76.4		
			968.5	4.35		
			1529.4	7.3		
^{108}In → ^{108}Cd	58.0 min	EC, β^+ (100)	242.6	41		
			325.6	13.7		
			511.0	50		
			632.9	100		
			875.4	100		
^{111m}Cd	48.5 min	IT (100)	**150.8**	29.1	^{112}Cd (p, d)	7.24
			245.4	94	^{112}Cd (p, pn)	9.48

These activity levels resulted from a total proton accumulated fluence equivalent to ~22 years mission fluence. Therefore, when scaling background noise level generated by these short-lived radioisotopes to the average background generated during one day we obtain ~1.3×10^{-5} at 100 keV down to ~2.5×10^{-6} counts/cm^2 s keV at 800 keV. In the same energy range, the in-orbit flux of a strong source gamma-ray emitter such as the Crab Nebula is of about ~10^{-2} photons/cm^2 s keV. Even considering the additional contribution of long-lived component activation which has a cumulative effect but generates lower background flux than short-lived, the activation background noise generated within the CdTe remains at a low level compared with main gamma-ray source emissions, as the Crab Nebula emissions. Furthermore, we are considering a highly conservative scenario, since high-energy observatory missions are equipped with passive shielding and collimators that reduce considerably the proton flux (ex.: 800 μm of tungsten stop totally 25 MeV protons). However, additional X- and gamma-rays background

Table 3
Characteristics of the main iodine radioisotopes generated by the irradiation of natural Cadmium by 14 MeV protons, ordered by decreasing cross-sections [18–20,23,24]. Whenever the decay daughter-nuclide is not stable, its characteristics are also presented.

Radioisotope	Half-life, $T_{1/2}$	Decay-mode (%)	Energy, E_γ (keV)	Yield per disintegration, I_γ (%)	Nuclear reactions	Threshold (MeV)
$^{125}I \to {}^{125}Te$	59.4 d	EC (100)	35.5	6.7	^{125}Te (p, n)	0.98
					^{126}Te (p, 2n)	10.16
$^{124}I \to {}^{124}Te$	4.176 d	EC, β^+	511.0	45.8	^{124}Te (p, n)	3.97
		(100)	**602.7**	62.9		
			722.8	10.4	^{125}Te (p, 2n)	10.60
			1691	11.2		
$^{123}I \to {}^{123}Te$	13.22 h	EC (100)	**159.0**	83.3	^{123}Te (p, n)	2.03
			529.0	1.4	^{124}Te (p, 2n)	11.54
$^{126}I \to {}^{126}Te$	12.93 d	EC, β^+	511.0	2.0		
		(52.7)	**666.3**	32.9		
			753.8	4.2	^{126}Te (p, n)	2.96
$\to {}^{126}Xe$		β^- (47.3)	**388.6**	35.6		
			491.2	2.9		
$^{128}I \to {}^{128}Xe$	24.99 min	β^- (93.1)	**442.9**	93.1		
			526.6	8.9	^{128}Te (p, n)	2.05
			969.5	2.2		
$\to {}^{128}Te$		EC (6.9)	–	–		
$^{130}I \to {}^{130}Xe$	12.36 h	β^- (100)	**417.9**	34.2		
			536.1	99		
			668.5	96	^{130}Te (p, n)	1.21
			739.5	82		
			1157.4	11.3		
			–	–		
$^{130m}I \to {}^{130}I$	8.84 min	IT (84)	536.1	15.7		
$\to {}^{130}Xe$		β^-(16)	586.0	1.07		
$^{121}I \to {}^{121}Te$	2.12 h	EC, β^+	**212.2**	84.3		
		(100)	511.0	21.2	^{122}Te (p, 2n)	12.98
			532.1	6.1		
$^{121}Te \to {}^{121}Sb$	19.17 d	EC (100)	507.6	17.7		
			573.1	80.4		

Table 4
Proton beam (~14 MeV, ⌀18 mm) irradiation settings for CdTe internal activation and radiation damage measurements. The total duration of the four irradiations sequence was ~4 h.

	Irradiation 1	Irradiation 2	Irradiation 3	Irradiation 4
Flux (protons/cm² s)	2.4×10^7	2.7×10^7	3.3×10^7	3.6×10^7
Irradiation time (s)	90	90	390	722
Total fluence (protons/cm²)	2.2×10^9	4.6×10^9	1.9×10^{10}	4.5×10^{10}
Equivalent time in orbit (years)	~1	~2.2	~9	~22

Table 5
Operational characteristics of the CdTe detector operated at room temperature and 600 V.

Active area - A	~0.16 cm²
Leakage current density - $I_{leakage}/A$	0.51 ± 0.08 μA/cm²
Equivalent noise charge	595 ± 8 e⁻
Energy resolution	12.6 ± 0.4% @ 122 keV
	4.6 ± 0.2% @ 511 keV
	2.3 ± 0.2% @ 1275 keV

noise is generated by the interaction of protons in these materials. We must consider as well the role of active shielding systems, such as anti-coincidence scintillators mounted on the perimeter and bottom of the detection plane. For example, SPI (SPectrometer for INTEGRAL) anticoincidence system on board INTEGRAL can provide background noise rejection rates that go from 3% for continuum noise up to ~100% for numerous background noise peaks [25]. Finally, reconstruction analysis software, based on Compton and pair production kinematics, provides photon's trajectory reconstruction levels up to ~40% in this energy range [26], contributing substantially for background noise events' rejection. Overall, these solutions contribute to minimize all the components of the background noise, specially the activation background generated by protons. Background reduction might reach one or more orders of magnitude, depending of the instrument final design and background reduction solutions.

4. Radiation damage

The assessment of radiation damage effects generated by LEO protons on a CdTe detector were analyzed by measuring its energy resolution degradation as well as monitoring its leakage current, when the proton irradiation fluence was increased up to an accumulated orbital proton fluence equivalent to a long duration mission (~22 years). Moreover, the energy resolution and the leakage current were measured one year later to evaluate the CdTe crystal recovery potential.

Before ICNAS proton beam irradiation, preliminary measurements were performed on the CdTe detectors in ICNAS facility environment. Firstly, ICNAS facility environment background level was measured. Afterwards, CdTe prototype's operational characteristics were determined: the leakage current, the equivalent noise charge and the energy resolution. The leakage current test was performed with a grounded Keithley 617 electrometer, applying the bias voltage to the CdTe cathode electrode with the 64 pixels interconnected [27]. The measured operational characteristics are summarized in Table 5.

4.1. Proton damage after irradiation

The CdTe prototype was then submitted to a series of 4 progressive irradiation doses, as described in Table 4. Figs. 7 and 8 show that the energy resolution degradation was negligible up to ~2.2 years'
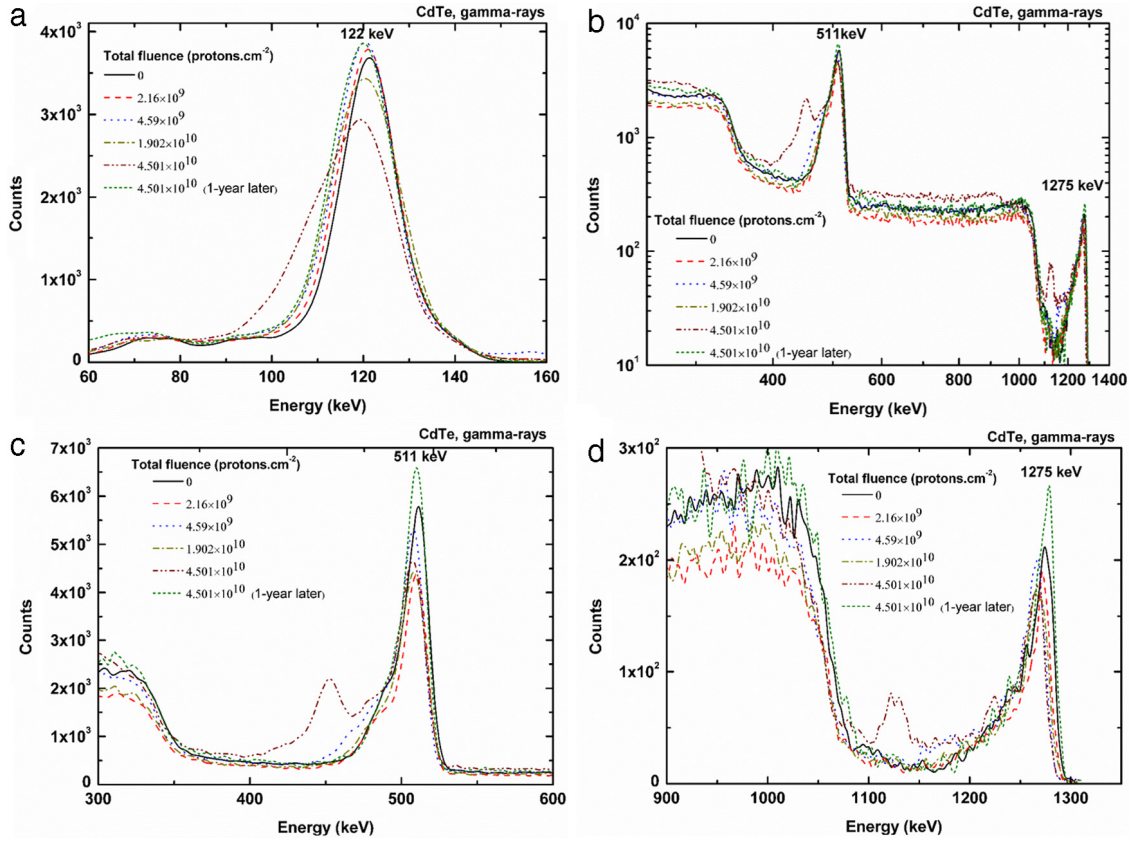
Fig. 5. CdTe matrix activation emission spectra measured with the HPGe detector after the irradiation settings A_2 (a and b) and A_3 (c and d). For A_2 irradiation, the two spectra were measured within the time-frame of ~10 to ~15 min and ~1 to ~4.3 h, after irradiation (14 MeV protons, total fluence 5.09×10^{10} protons/cm²). For A_3 irradiation, the two spectra were measured within the time range ~5.0 to ~5.6 h and ~43 to ~43.3 h, after irradiation (14 MeV protons, total fluence 5.41×10^{13} protons/cm²). The identified radioisotopes are indicated.

Fig. 6. CdTe detector internal activation emission spectra after Irradiation 1 (a) and 4 (b). For Irradiation 1, the spectra were measured ~15 to 22 min, ~22 to 37 min, ~37 to 55 min and ~15 to 55 min, after irradiation (total fluence: 2.16×10^9 protons/cm²). For Irradiation 4, the spectra were measured ~15 to 35 min, ~35 to 45 min, ~45 to 60 min and ~15 to 60 min, after irradiation (total fluence: 4.50×10^{10} protons/cm²)

equivalent dose. Degradation becomes perceptible in case of proton fluence equivalent to a LEO mission duration of ~9 years and it further deteriorates up to ~22 years dose, when the energy resolution deteriorates by 60% when compared with the initial value at 122 keV. Since a 22 years fluence equivalent is an estimation for a long duration scientific mission, these results show that the cumulative dose can potentially deteriorate the energy resolution of a CdTe based instrument. However, the degradation only becomes significant for a period longer than 10 years and especially for lower energy gamma-ray measurements. For higher energies (>500 keV) performance deterioration is limited (<20%

deterioration) and still allows acceptable performances for most of the mission duration. At Irradiation 4 fluence level, we registered a small peak in the spectra at about 10% lower energy than both the 511 and 1275 keV peaks. It can be explained by a hole trapping channel inside the material that was definitively opened for irradiation 4 – note that there is already a slight tendency for trapping for lower doses.

The energy resolution deterioration trends herein obtained are similar to those obtained by other authors with CdTe detectors for other proton energies [13,15,16], as well as for 15 MeV [14], however in this last experiment the dose delivered was lower (1.3×10^9 protons/cm²),

Fig. 7. CdTe prototype energy spectra obtained after different fluence levels of ICNAS proton beam irradiation for: (a) [57]Co and (b) [22]Na radioactive sources. In (c) and (d), the [22]Na 511 keV and 1275 keV emission lines spectrum, respectively, are represented in more detail. Spectra obtained one year later for the same prototype are also represented.

approximately of the order of the stronger solar burst of 1972. Obviously, in our experiment we simulate a ∼22 years' dose given in a very short period (few minutes) which causes increased energy resolution degradation at short term. It is expected that the same dose irradiating a CdTe detection plane during 22 years – with stronger intensity at each crossing in the SAA – allows material properties to recover at a certain extent. Furthermore, in a space mission, shielding passive elements are not distributed homogeneously around the detection plane and different proton orientation angles and irradiation sites generate special asymmetric detector performance degradation. As referred in Section 3, the average range for the 14 MeV beam protons is 0.81 mm. Hence, most of the ICNAS beam protons were stopped between the surface and the middle of the prototype and all proton energy was deposited inside the detector. The deposited energy density within the crystal is correlated with the deterioration of its charge transport properties due to the charge trapping sites generated by the protons [28]. Charge trapping causes a variation of the charge collection efficiency with the crystal depth, resulting in the deterioration of the energy resolution. However, as discussed in the previous chapter, the deposited energy density inside the crystal will be lower for proton energies from 25 MeV (mean range ∼2 mm) up to 300 MeV. Consequently, 14 MeV is a fairly representative proton beam energy also to study the proton damage effects on such 2 mm thick CdTe detector.

4.2. Proton damage one year later

The first week of July 2016, one year after the ICNAS prototype proton irradiation experiment (July 2015), we measured the energy resolution of the same CdTe prototype for the same set of energies (122, 511 and 1275 keV). In the meanwhile, this prototype was kept inside a laboratory locker at room temperature, away from solar or artificial illumination. In Figs. 7 and 8 are also represented the spectra and the

energy resolutions obtained one year after the prototype irradiation. As can be seen, the energy resolution improved for all the measured energy lines. The recovery was nearly total for high-energy lines. For the 122 keV line the energy resolution recovered down to ∼15% above the initial resolution, before the irradiation. This result means that the CdTe crystalline structure properties show a certain level of recovery capability one year later. Indeed, at room temperature the material structure acquires enough energy for a certain extent of lattice recovery to its initial state, which is reflected in the energy resolution improvement. However, it is not a full recovery, indicating that some irreversible effects remain in the material structure after proton irradiation, if no further treatment is applied on the detector. For instance, in some space mission payloads there is some limited material structure treatment and recovery capability, such as thermal annealing cycles [3,29]. In Fig. 7, it is also noticeable a slight increment in recorded counts one year later for the same acquisition time. This can be easily explained by the slight differences in the irradiation geometry and orientation of the radioactive sources when the system was set one year later.

Furthermore, the prototype leakage current was measured for the entire pixelized matrix one year later (0.66 μA/cm²), however no significant current variation was observed, remaining within a ±20% range.

In other authors' similar experiment [17] where measurements were also performed one year later, it is reported that the material recovered, however no quantification or details are given about the recovery and the radiation damage immediately after the irradiation provides also limited conclusions.

5. Conclusions

A CdTe prototype for high-energy astrophysics, when irradiated by a 14 MeV proton beam, generated nuclear activation spectra dominated by indium and iodine radioisotopes. Most of the radioactive
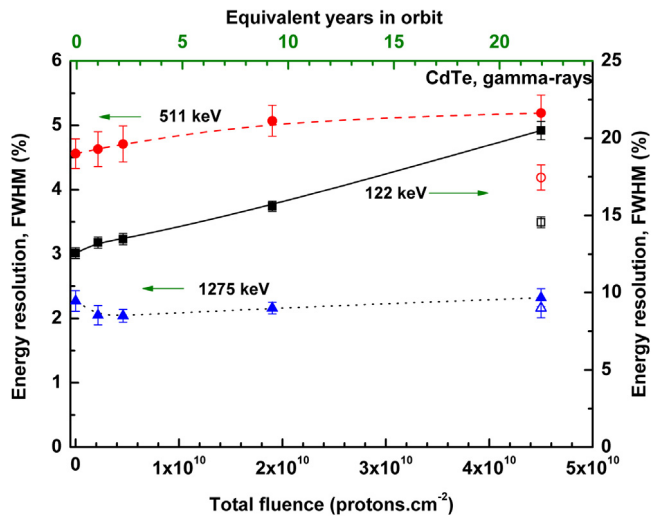
Fig. 8. Prototype energy resolution degradation for ^{57}Co 122 keV (right vertical axis) and for ^{22}Na 511 keV and 1274 keV peaks (left vertical axis), after its irradiation by a 14 MeV protons beam up to 4.5×10^{10} protons cm^{-2} total fluence. Open symbols correspond to measurements performed one year later for the same emission lines.

isotopes were successfully identified, providing useful data for inflight background noise reduction methods. Prototype external and internal measurements show low activation background level ($<1.3 \times 10^{-5}$ counts/cm^2 s keV scaled for 1 day LEO protons and short-lived radioisotopes) compared with the emission level of main gamma-ray sources such as the Crab Nebula, when irradiated by proton fluences equivalent to scientific mission time-frames up to ~22 years. Furthermore, a CdTe based high-energy space telescope equipped with passive and active (anti-coincidence) shielding will reduce one or more orders of magnitude proton nuclear activation component. Therefore, we can fairly estimate that the contribution of CdTe activation background should have a minimal impact in instruments' performance deterioration.

Furthermore, CdTe presents good radiation hardness for typical LEO proton fluences. The measured energy resolution shows a small degradation up to 9 years orbital proton fluence equivalent, but for lower energies (122 keV) and 22 years equivalent proton fluence the energy resolution deteriorates by 60%, however it is still suitable for most of the mission scientific requirements. For 511 keV the energy resolution degradation is about 14%, becoming lower for higher gamma-ray energies. Furthermore, CdTe show a very good level of spectroscopic properties' recovery, actually one year after the irradiation the energy resolution recovered almost totally for higher energies (e.g. 511 and 1275 keV) and recovered down to an energy resolution level only ~15% worse before proton irradiation for the 122 keV line.

Acknowledgments

References

[1] R. Terrier, et al., In-flight calibration of the ISGRI camera, Astron. Astrophys. 411 (2003) 167.

[2] J.B. Stephen, et al., The in-flight background of IBIS/PICsIT, Astron. Astrophys. 411 (2003) 203.

[3] F. Lebrun, et al., INTEGRAL: In flight behavior of ISGRI and SPI, Nucl. Instrum. Methods Phys. Res. A 541 (2005) 323.

[4] N. Auricchio, et al., Development of a CZT spectroscopic 3D imager prototype for hard X ray astronomy, in: IEEE Nuclear Science Symposium and Medical Imaging Conference, 2013 NSS/MIC, Seoul, 2013. http://dx.doi.org/10.1109/NSSMIC.2013.6829832.

[5] J. Knödlseder, et al., GRI: focusing on the evolving violent universe, in: S. L. O'Dell and G. Pareschi (Eds.), SPIE Proceedings on Optics for EUV, X-ray, and Gamma-Ray Astronomy III, vol. 6688, 2007, p. 668806.

[6] T. Takahashi, et al., The ASTRO-H Mission, in: M. Arnaud, S. S. Murray and T. Takahashi (Eds.), SPIE Proceeding on Space Telescopes and Instrumentation 2010: Ultraviolet to Gamma Ray, Vol. 7732, 2010, p. 77320Z.

[7] D.M. Sawyer, J.I. Vette, AP-8 Trapped Proton Environment for Solar Maximum and Solar Minimum, National Space Science Data Center, National Aeronautics and Space Administration, Goddard Space Flight Center, NASA-TM-X-72605, 1976.

[8] C.E. Jordan, NASA radiation belt models AP-8 and AE-8, RADEX, Inc. Bedford, MA, Scientific Report No. 1, GL-TR-89-0267, 1989.

[9] J.I. Vette, The NASA/National Space Science Data Center: Trapped Radiation Environment Model Program (1964-1991), National Space Science Data Center, World Data Center A for Rockets and Satellites, NASA, Goddard Space Flight Center, SDC/WDC-A-R&S 91-29, 1991.

[10] N.V. Kuznetsov, N.I. Nikolaeva, Trapped proton fluxes measured on board LEO satellites in comparison with models, Adv. Space Res. 45 (2010) 1315.

[11] OMERE: Outil de Modélisation de l'Environnement Radiatif Externe, http://www.trad.fr/OMERE-14.

[12] R. Silberberg, C.H. Tsao, Cross sections for (p, xn) reactions and astrophysical applications, Astrophys. J. Suppl. 35 (1977) 129.

[13] M. Zanarini, et al., Radiation damage induced by 2 MeV protons in CdTe and CdZnTe semiconductor detectors, Nucl. Instrum. Methods Phys. Res. B 213 (2004) 315.

[14] F. Lebrun, C. Blondel, I. Fondeur, A. Goidwurm, P. Laurent, J.-P. Leray, ISGRI : A CdTe array imager for INTEGRAL, in: Proc. SPIE, vol. 2806, 2, 1996, pp. 258–268.

[15] Y. Eisen, L.G. Evans, S. Floyd, C. Schlemm, R. Starr, J. Trombka, Radiation damage of Schottky CdTe detectors irradiated by 200 MeV protons, Nucl. Instrum. Methods A 491 (2002) 176–180.

[16] M.M. Murakami, et al., Activation properties of Schottky CdTe diodes irradiated by 150 MeV protons, IEEE Trans. Nucl. Instrum. 50 (4) (2002) 1013–6 1019.

[17] O. Limousin, et al., ASTRO-H CdTe detectors proton irradiation at PIF, Nucl. Instrum. and Meth. Phys. Res. A 787 328-335.

[18] M.U. Khandaker, K. Kim, M.W. Lee, K.S. Kim, G.N. Kim, Y.S. Cho, Y.O. Lee, Production cross-sections for the residual radionuclides from the natCd(p, x) nuclear processes, Nucl. Instrum. Methods Phys. Res. B 266 (2008) 4877–4887.

[19] F. Tárkányi, et al., Activation cross-sections on cadmium: Proton induced nuclear reactions up to 80 MeV, Nucl. Instrum. Methods Phys. Res. B 245 (2006) 379–394.

[20] K.M. El-Azony, et al., Proton induced reactions on natural tellurium up to 63 MeV: Data validation and investigation of possibility of I-124 production, Radiochim. Acta 96 (2008) 763–769.

[21] S. Ghithan, et al., Development of a PET Cyclotron Based Irradiation Setup for Proton Radiobiology, JINST 10 P02010, 2015.

[22] J.F. Ziegler, J. Biersack, U. Littmark, The Stopping and Range of Ions in Matter, Pergamon Press, 1985.

[23] Robert M. Bruckner, Roland Braito, QTool Documentation, IFS Technical Report, January 2003.

[24] Alejandro Sonzogni, NuDat, a nuclear structure and decay data searchable database, in: Division of Nuclear Physics Meeting, American Physical Society, Chicago, 2004, pp. 27–30.

[25] P. Jean, et al., SPI instrumental background characteristics, Astron. Astrophys. 411 (2003) L107–L112.

[26] A. Zoglauer, R. Andritschke, F. Schopper, MEGAlib –The medium energy gamma-ray astronomy library, New Astron. Rev. 50 (20) (2006) 629–632.

[27] J.M. Maia, R.M. Curado da Silva, Yoon-Seong Kim, Yoon-Seong Kim prospects on low-Z elements K fluorescence and actinide-radionuclides L fluorescence X-ray detection with cooled CZT, IEEE Trans. Nucl. Sci. 62 (2) (2015) 577–586.

[28] Beatrice. Fraboni, et al., Deep traps induced by 700 keV protons in CdTe and CdZnTe detectors, Trans. Nucl. Sci. 54 (2007) 4.

[29] G. Vedrenne, et al., SPI: The spectrometer aboard INTEGRAL, Astron. Astrophys. 411 (1) (2003) 63–70.